

# Slow dynamics and precursors of the glass transition in granular fluids

Iraj Gholami,<sup>1,\*</sup> Andrea Fiege,<sup>2,1</sup> and Annette Zippelius<sup>1,2</sup>

<sup>1</sup>*Georg-August-Universität Göttingen, Institut für Theoretische Physik,  
Friedrich-Hund-Platz 1, D-37077 Göttingen, Germany*

<sup>2</sup>*Max-Planck-Institut für Dynamik und Selbstorganisation, Bunsenstr. 10, D-37073 Göttingen, Germany*

We use event driven simulations to analyze glassy dynamics as a function of density and energy dissipation in a two-dimensional bidisperse granular fluid under stationary conditions. Clear signatures of a glass transition are identified, such as an increase of relaxation times over several orders of magnitude. As the inelasticity is increased, the glass transition is shifted to higher densities and the precursors of the transition become less and less pronounced – in agreement with a recent mode-coupling theory. We analyze the long-time tails of the velocity autocorrelation and discuss its consequences for the nonexistence of the diffusion constant in two dimensions.

PACS numbers: 45.70.-n, 47.10.-g, 05.20.Jj

## I. INTRODUCTION

The physics of nonequilibrium systems in general involves dissipation and energy injection. These properties distinguish nonequilibrium but stationary systems from those in thermodynamic equilibrium and render the application of standard thermodynamics and statistical mechanics impossible such that one has to develop new methods to treat nonequilibrium systems or resort to experimental and computational methods. Due to their inherent dissipative nature, driven granular fluids serve as model systems for nonequilibrium phenomena and in particular phase transitions in macroscopic systems out of equilibrium. Questions addressed include the crystallization of granular fluids [1, 2], the jamming transition [3] and the glass transition [4].

Here we focus on a two-dimensional driven granular fluid, displaying structural arrest as the density is increased. Most experimental work in the field does indeed use a two-dimensional setup, allowing for extensive particle tracking with high speed and resolution cameras. Several driving mechanisms have been studied, such as vertical vibrations [1, 2, 5] and air-tables [6–8]. Since we are interested in structural arrest, the most relevant experiments are those of Abate and Durian [6, 7], who showed that the approach to jamming in a granular medium resembles the glass transition in a molecular or colloidal fluid: The mean square displacement develops a plateau and the dynamics becomes strongly heterogeneous.

Recently a mode-coupling theory [4] has been set up for a driven granular fluid in the stationary state. A glass transition was located below random close packing which is qualitatively similar, but quantitatively different from the corresponding transition for a molecular fluid. The coherent scattering function was shown to display a plateau – provided the density is sufficiently close to the glass transition. The timescale for relaxation from the

plateau ( $\alpha$ -relaxation) diverges at the glass transition. The transition density as well as the dynamics depend on the degree of inelasticity, parametrized by the coefficient of restitution.

In this paper we investigate the dynamics of a driven two-dimensional granular fluid close to the glass transition, mimicking an air-table experiment. We use event driven simulations to compute the mean square displacement, the velocity autocorrelation, and the incoherent scattering function.

## II. MODEL

Dense systems of monodisperse, elastic hard disks are known to undergo a phase transition to a crystalline state [9]. The only state variable is the packing fraction  $\eta$ , defined by the area covered by particles divided by the area of the whole system. The phase transition occurs for packing fractions between  $\eta_f = 0.691$  and  $\eta_s = 0.7163$ , where packing fractions up to  $\eta_f$  are completely in the fluid phase and packing fractions larger than  $\eta_s$  are completely in the solid phase. Packing fractions between  $\eta_f$  and  $\eta_s$  fall into the coexistence area. An overview over simulations performed to determine the phase transition is given in [10]. Crystallization can be avoided in binary mixtures of particles with sufficiently different sizes. Whereas bidisperse mixtures of elastic hard spheres form stable crystalline structures for a size ratio smaller than 1.2 [11], larger size ratios suffice to avoid crystallization. We expect similar behaviour for a granular fluid and choose a bidisperse symmetric mixture of hard disks. The ratio of the radius of the big particles,  $R_b$ , to the radius of the small particles,  $R_s$ , is given by  $R_b/R_s = 1.43$ .

### A. Collision rules

We restrict our analysis to smooth particles without rotational degree of freedom. Particles' positions and velocities are denoted by  $\{\mathbf{r}_i, \mathbf{v}_i\}_{i=1}^N$ . The dissipation arises

\*Author to whom correspondence should be addressed.  
iraj.gholami@theorie.physik.uni-goettingen.de

solely from incomplete normal restitution with a constant coefficient of restitution  $\varepsilon$ : The change of the relative velocity  $\mathbf{g} := \mathbf{v}_1 - \mathbf{v}_2$  in the direction of the normal vector  $\mathbf{n} := (\mathbf{r}_1 - \mathbf{r}_2)/|\mathbf{r}_1 - \mathbf{r}_2|$  is given by

$$(\mathbf{g} \cdot \mathbf{n})' = -\varepsilon(\mathbf{g} \cdot \mathbf{n}). \quad (1)$$

Here primed and unprimed quantities indicate postcollisional and precollisional velocities of the two colliding particles. The postcollisional velocities of the two colliding disks are expressed in terms of the precollisional velocities according to

$$m_1 \mathbf{v}'_1 = m_1 \mathbf{v}_1 - \delta, \quad (2)$$

$$m_2 \mathbf{v}'_2 = m_2 \mathbf{v}_2 + \delta, \quad (3)$$

where

$$\delta = \frac{m_1 m_2}{m_1 + m_2} \frac{1 + \varepsilon}{2} (\mathbf{g} \cdot \mathbf{n}) \mathbf{n}. \quad (4)$$

Here  $m_i$  denotes the mass of particle  $i$  and we assume constant mass density for all particles such that the mass ratio of the big to the small particles is given by  $(R_b/R_s)^2$ .

### B. Driving

Due to inelastic collisions, energy is dissipated and we have to feed energy into the system in order to obtain a stationary state. One of the simplest driving mechanisms [12] is to kick a given particle, say, particle  $i$ , instantaneously at time  $t$  according to

$$\mathbf{p}'_i(t) = m_i \mathbf{v}'_i(t) = \mathbf{p}_i(t) + p_{\text{Dr}} \boldsymbol{\xi}_i(t). \quad (5)$$

Here  $p_{\text{Dr}}$  is the driving amplitude and  $\boldsymbol{\xi}_i(t)$  indicates the direction of the driving which is chosen randomly with  $\langle \xi_i^\alpha(t) \xi_j^\beta(t') \rangle = \delta_{ij} \delta_{\alpha\beta} \delta(t - t')$ . The Cartesian components  $\xi_i^\alpha$ ,  $\alpha = x, y$ , are distributed according to a Gaussian distribution with zero mean.

In practice, we implement the stochastic driving process by kicking the particles randomly with frequency  $f_{\text{Dr}}$ . In order to conserve momentum locally, we apply kicks of equal magnitude and opposite direction to pairs of neighbouring particles [13]. Thereby momentum is conserved locally.

### C. Implementation

As long as the system is not jammed, the collisions of hard particles are instantaneous, so that event driven simulations can be applied. Lasting contacts, that we expect to occur in a jammed state, cannot be accounted for by event driven simulations, so that we are restricted to densities below the jamming point. The glass transition in a driven granular fluid is expected to occur at densities below jamming, so that the restriction is actually less severe.

We use an efficient standard event driven algorithm [14] that enables us to simulate large systems for long times. Inelastically colliding hard particles are known to undergo the so-called *inelastic collapse*. We circumvent the inelastic collapse with the same method used in [15].

We consider a system of  $N = 10000$  particles in an area  $A = L^2$ , where  $L$  denotes the length of system. The mixture is chosen symmetric, so that small and big particles appear in equal numbers. Initial velocities are drawn from a Gaussian distribution. To analyze the slow dynamics of the system as the glass transition is approached, we simulate a range of coefficients of restitution,  $0.5 < \varepsilon < 0.95$  and area fractions  $0.1 \leq \eta \leq 0.81$ . For every parameter set  $(\eta, \varepsilon)$  we performed an event driven molecular dynamic simulation with approximately  $10^7$  collisions per particle.

Several initial configurations with  $\eta = 0.84$  were taken from a time driven molecular dynamics simulation of soft disks [16], that suffer dissipation and finally come to rest. By expanding the system we change the packing fraction, allowing us to investigate systems of hard disks up to  $\eta = 0.81$ . To be sure that our simulations do not depend on the initial configurations (*i.e.*, the initial values of particles' velocities and positions), we have repeated the simulation for each parameter set, using several different initial configurations.

In order to investigate the long-time behaviour of the mean square displacement and the velocity autocorrelation function it was necessary to simulate larger systems with  $N = 4 \cdot 10^6$ . This was done for  $\varepsilon = 0.7, 0.8, 0.9$  and  $\eta = 0.1 \dots 0.78$ .

## III. RESULTS

Our main concern is the slow dynamics in a dense granular fluid and in particular the precursors of the glass transition. Our analysis will be based on the time dependent van Hove correlation function, the mean square displacement (MSD) and the velocity autocorrelation function (VACF) in the *stationary* state. Hence we briefly regress to discuss the relaxation towards stationarity.

### A. Stationary state

To maintain a stationary state, the dissipated energy due to inelastic collisions must be compensated by a comparable driving energy fed into the system. In a two-dimensional monodisperse system, we define the granular temperature as the average kinetic energy

$$T := \frac{1}{N} \sum_{i=1}^N \frac{m}{2} \mathbf{v}_i^2. \quad (6)$$

A stationary state can be achieved by balancing dissipation and driving [17]

$$0 = \frac{dT}{dt} = \left. \frac{dT}{dt} \right|_{\text{Drive}} + \left. \frac{dT}{dt} \right|_{\text{Inelastic}} \approx f_{Dr} \frac{p_{Dr}^2}{2m} - \omega_E \frac{1 - \varepsilon^2}{4} T. \quad (7)$$

The collisional loss is estimated by the energy loss in a single collision,  $\frac{1 - \varepsilon^2}{4} T$ , multiplied by the Enskog collision frequency  $\omega_E$ :

$$\omega_E = 2\pi g(2a)(2a)^{d-1} \frac{N}{A} \sqrt{\frac{T(t)}{\pi m}}. \quad (8)$$

Here  $g(2a)$  is the pair correlation at contact.

In the following we are going to discuss correlations, such as the MSD or the VACF as a function of density and inelasticity  $\varepsilon$ . We are particularly interested in the approach to the glass transition as the inelasticity is varied. To isolate effects of inelasticity and packing fraction, we have to keep the temperature constant (without loss of generality we take  $T \sim 1$ ). This can be achieved approximately by adjusting the driving (see Eq. 7) according to

$$\Rightarrow p_{Dr} = \sqrt{\frac{1 - \varepsilon^2}{2} \frac{m\omega_E}{f_{Dr}}}. \quad (9)$$

In order to sustain a stationary state we choose the driving frequency of the order of the collision frequency as suggested by Bizon *et al.* [18]. Note that the driving amplitude scales with the coefficient of restitution, such that we are able to take the elastic limit,  $\varepsilon \rightarrow 1$ .

In a symmetric binary mixture, we define two temperatures, one for the big particles ( $T_b$ ) and one for the small ones ( $T_s$ ):

$$T_b = \frac{m_b}{N} \sum_i \delta_{R_i, R_b} v_i^2$$

$$T_s = \frac{m_s}{N} \sum_i \delta_{R_i, R_s} v_i^2. \quad (10)$$

These are in general unequal in the stationary state due to violation of equipartition [19]. The analogous cooling equations for  $T_b$  and  $T_s$  have been derived, also in the presence of driving, and can in principle be used to determine the driving amplitude [20]. We refrain from an exact solution and instead choose the driving amplitude  $p_{Dr} \sim \sqrt{1 - \varepsilon^2}$  and absorb the density dependence in  $f_{Dr}$  which is chosen equal to the collision frequency. An example for the relaxation to the stationary state is shown in Fig.1, where we plot the two temperatures  $T_b$  and  $T_s$ .

In the following we use units of length, mass and time, such that the radius of the small particles is one, their mass is one and  $\frac{1}{2} m_i v_i^2(t=0) = 1$  (average over all particles). The natural time step in an event driven simulation is the number of collisions. In the stationary state the

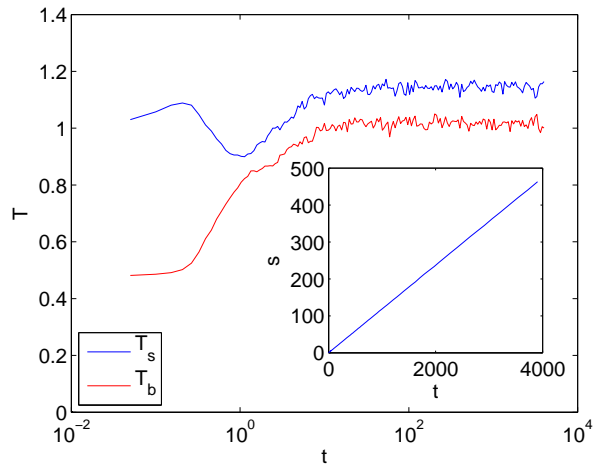


FIG. 1: (Color online) Time dependence of the temperature of the small particles ( $T_s$ , upper curve) and big particles ( $T_b$ , lower curve) for  $\varepsilon = 0.90$  and packing fraction  $\eta = 0.5$ . Inset: Number of collisions per particle  $s$  as a function of time in dimensionless units.

number of collisions increases linearly in time, as shown in the inset of Fig. 1 so that the two are related by a constant factor.

## B. Long-time tails of the Velocity Autocorrelation

The VACF is defined by

$$\Phi(t) = \frac{1}{N} \sum_{i=1}^N \langle \mathbf{v}_i(t) \mathbf{v}_i(0) \rangle, \quad (11)$$

where the average  $\langle \dots \rangle$  is taken over initial conditions. The VACF is known to exhibit a hydrodynamic long-time tail in systems of hard spheres [21, 22] and hard disks [23]. Such long-time tails have also been observed in driven granular fluids in three dimensions. It was furthermore shown by simulations and a simple scaling argument that the tails depend sensitively on the driving mechanism: If driving conserves momentum locally, then the  $t^{-3/2}$ -tail known from elastic systems prevails, whereas it is replaced by  $t^{-1}$ , if momentum is not conserved by the driving [15].

For two-dimensional fluids the situation is less clear. Two functional forms of the long-time decay of the equilibrium VACF have been proposed. Hydrodynamic theory [24] as well as mode-coupling theory [25] predict  $\Phi_{HD} \propto t^{-1}$ . If these approaches are made self-consistent [26, 27], the time decay is changed to  $\Phi_{SC} \propto t^{-1} (\sqrt{\ln(t)})^{-1}$  in agreement with renormalization group theory [28]. Recent simulations [23] claim that the self-consistent theory is supported by large scale simulations.

We compute the VACF for a bidisperse mixture of  $N = 4 \cdot 10^6$  particles as suggested by [23] in order to

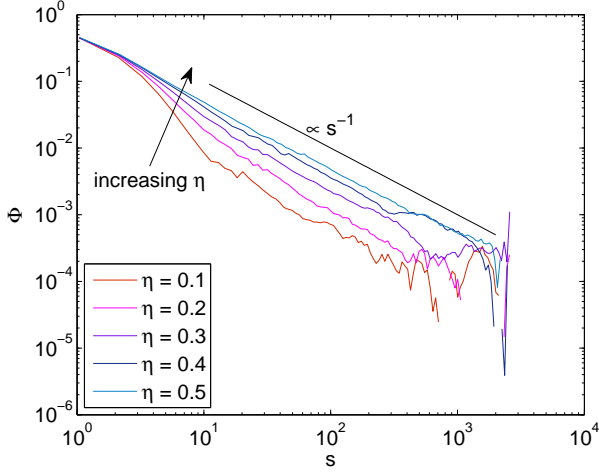


FIG. 2: (Color online) The VACF for small particles for low and intermediate packing fractions as a function of time measured in number of collisions per particle  $s$ . The long-time tails are more pronounced for increasing  $\eta$ .

be able to analyze the long-time behavior of the VACF. The more inelastic system,  $\varepsilon = 0.7$ , is expected to exhibit the most prominent long-time tail as observed in three-dimensional inelastic fluids [15]. Fig. 2 shows the VACF for an inelastic mixture with  $\varepsilon = 0.7$  and packing fractions up to  $\eta = 0.5$ . The long-time tail in the decay seems to be most pronounced for  $\eta = 0.4$  and  $\eta = 0.5$ . In order to test the above predictions, we divide the VACF by each of the suggested decay laws and show the result in Fig. 3. If one of the two decay laws described the decay exactly, then the resulting curve should fluctuate around a constant. This is not the case neither for  $\propto t^{-1}$  nor for  $\propto t^{-1} \sqrt{\ln(t)}$ . Hence, neither of the suggestions is supported by our data, however we cannot exclude that one has to go to even longer times to identify the long-time tail unambiguously.

For increasing  $\varepsilon$  and high packing fractions the VACF is expected to show backscattering effects, *i.e.*, a time interval, in which the VACF becomes negative because the particles are reflected from the cage formed by their neighbours. This is confirmed by the VACF in a system of  $\eta = 0.72$  where the negative part of the VACF sets in for larger  $\varepsilon$  after showing a dip for intermediate  $\varepsilon$ , see Fig. 4. For constant  $\varepsilon$ , the range of the negative VACF is increased for increasing  $\eta$ , see inset of Fig. 4.

### C. Mean Square Displacement and Diffusion Coefficients

One prominent signature of the glass transition is the formation of a plateau in the MSD

$$\langle (\Delta \mathbf{r}(t))^2 \rangle = \frac{1}{N} \sum_i^N \langle (\mathbf{r}_i(t) - \mathbf{r}_i(0))^2 \rangle. \quad (12)$$

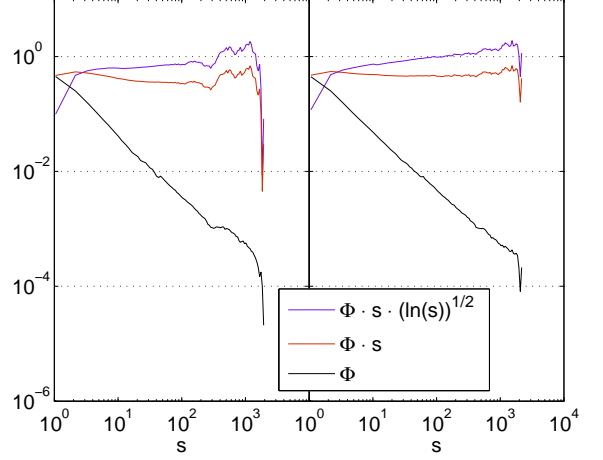


FIG. 3: (Color online) The VACF (lower curves) for small particles for  $\eta = 0.4$  (left) and  $\eta = 0.5$  (right) and  $\varepsilon = 0.7$ , divided by both predictions  $\Phi \propto s^{-1}$  (middle),  $\propto s^{-1}(\sqrt{\ln(s)})^{-1}$  (upper curves); time given in number of collisions per particle  $s$ .

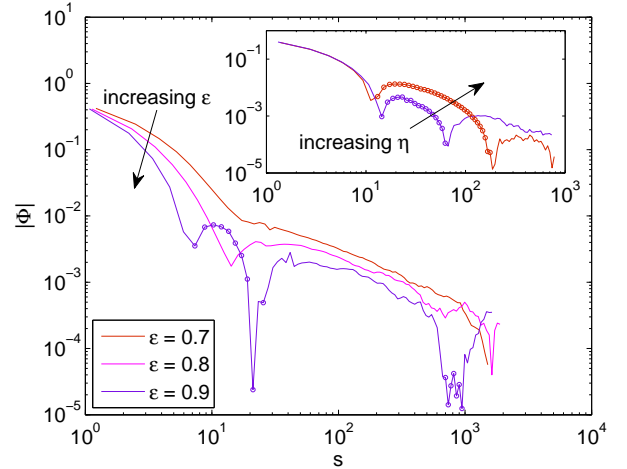


FIG. 4: (Color online) The VACF for small particles for different  $\varepsilon$  at packing fraction  $\eta = 0.72$ . Marked data points indicate a negative value. Inset: The VACF for  $\varepsilon = 0.7$  and packing fractions  $\eta = 0.76, 0.78$ ; time given in number of collisions per particle  $s$ .

The MSD for a mildly inelastic system (coefficient of restitution  $\varepsilon = 0.9$ ) is shown in Fig. 5 for a wide range of packing fractions  $0.1 \leq \eta \leq 0.81$ . The simulated system consists of 10000 particles, which have been simulated for  $10^7$  collisions per particle. Subsequently, the data was divided into approximately 1000 time intervals each of them giving rise to a single MSD. These were averaged to obtain the final time dependent MSD [29] with a standard error of  $3 \cdot 10^{-4}$ . Ballistic motion is observed for small times for all densities. The larger the density the smaller

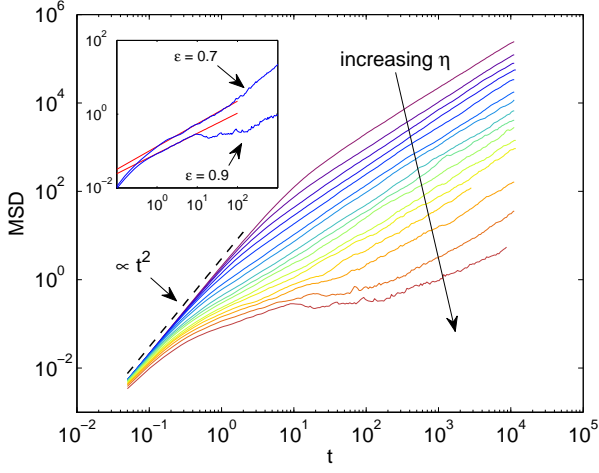


FIG. 5: (Color online) MSD for small particles for  $\varepsilon = 0.90$  and different packing fractions  $\eta = 0.1; 0.2; 0.3; 0.4; 0.5; 0.6; 0.65; 0.7; 0.72; 0.74; 0.75; 0.76; 0.77; 0.78; 0.79; 0.80; 0.81$ .

the ballistic regime. For packing fractions  $\eta < 0.7$ , ballistic motion crosses over to diffusive behaviour at long times. For  $\eta \geq 0.7$ , a plateau develops, indicating that a cage has formed which restricts the particles motion to the space within the cage. Actually, our data indicate subdiffusive behavior instead of a plateau; a blowup of the relevant time range is shown in the inset of Fig. 5. For times  $1 < t < 10$  the MSDs for  $\eta = 0.81$  show algebraic increase with exponents 0.6163(11) for  $\varepsilon = 0.7$  and 0.547(6) for  $\varepsilon = 0.9$ , respectively.

For area fraction  $0.7 \leq \eta \leq 0.77$  the cage is observed to break up for longer times so that ultimately diffusion prevails except for the highest density.

As the system becomes more inelastic we expect the glass transition to shift to higher densities [4]. Furthermore the range of densities where a clear separation of timescales can be observed, is expected to shrink. These expectations are indeed born out by our simulations. The MSD for a more inelastic system (coefficient of restitution  $\varepsilon = 0.7$ ) is shown in Fig. 6. The plateau is hardly visible as compared to the more elastic system, instead subdiffusive behaviour is observed for the highest densities.

Next, we want to quantify the prediction of granular mode-coupling theory (GMCT) that the more inelastic systems require increasing critical densities for the glass transition to occur. This is done in two steps. We first identify a timescale, such that the small particles' MSD = 1. This corresponds to the time at which the mean travelled distance of all small particles equals their radius. This timescale, i.e.  $t(\text{MSD} = 1)$ , is shown in Fig. 7 as a function of area fraction for a wide range of  $\varepsilon$ . As can be seen in the figure, this time scale strongly increases as the glass transition is approached, the more so the more elastic the system. Now we ask: at what

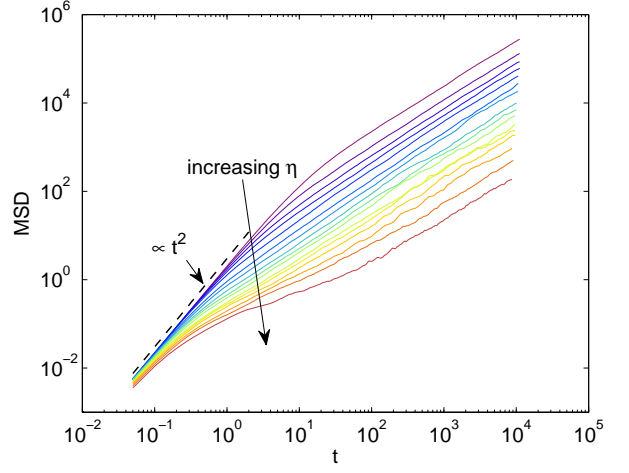


FIG. 6: (Color online) MSD for small particles for  $\varepsilon = 0.70$  and different packing fractions  $\eta = 0.1; 0.2; 0.3; 0.4; 0.5; 0.6; 0.65; 0.7; 0.72; 0.74; 0.75; 0.76; 0.77; 0.78; 0.79; 0.80; 0.81$ .

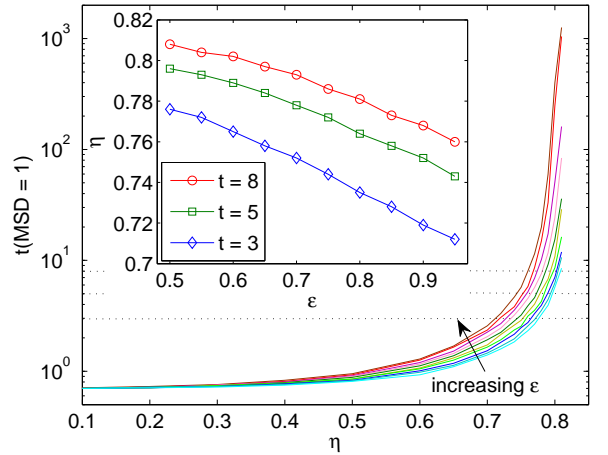


FIG. 7: (Color online) Times  $t(\eta, \varepsilon)$  of equal MSD for small particles for  $\varepsilon = 0.5, 0.55, 0.6, 0.65, 0.7, 0.75, 0.8, 0.85, 0.9, 0.95$ . Inset: Lines of equal MSDs for different times.

area fraction has the timescale acquired a given value, e.g.  $t(\text{MSD} = 1) = 3$ ? This yields an area fraction as a function of  $\varepsilon$ , which is shown as the blue curve in the inset and corresponds to the lowest broken line in the main part of the figure. Hence, in the inset we show lines of *equal relaxation time* ( $t = 3, 5, 8$ ) in the  $(\eta, \varepsilon)$  plane. For all times  $t$  the packing fraction  $\eta$  is a monotonically decreasing function of  $\varepsilon$  in agreement with GMCT [4].

The MSD is related to the VACF by  $\frac{\partial}{\partial t} \Delta \mathbf{r}^2(t) = 2 \int_0^t \Phi(t') dt'$ . With this relation we can define a time dependent diffusion coefficient  $D(t) := 1/2 \int_0^t \Phi(t') dt'$ . The predicted functional forms of the VACF,  $\Phi_{\text{HD}}(t) \propto t^{-1}$  and  $\Phi_{\text{SC}}(t) \propto t^{-1}(\sqrt{\ln(t)})^{-1}$ , respectively, yield the fol-

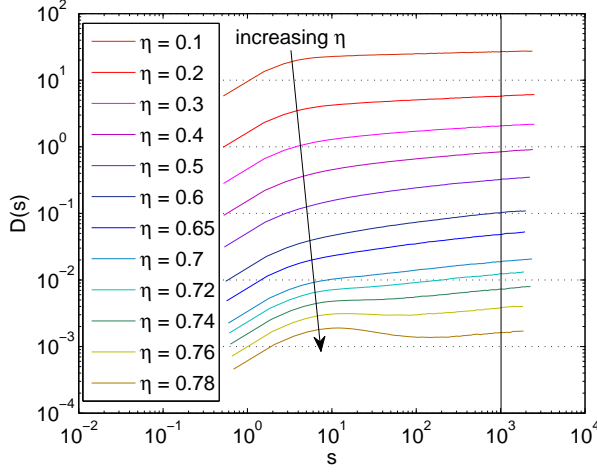


FIG. 8: (Color online) Time dependent diffusion coefficient  $D(s)$  for small particles for  $\varepsilon = 0.7$  and different packing fractions.

lowing time dependent diffusion coefficients:

$$D_{\text{HD}}(t) \propto \ln t, \quad (13)$$

$$D_{\text{SC}}(t) \propto \sqrt{\ln t}. \quad (14)$$

Both of these expressions diverge for  $t \rightarrow \infty$ , hence for both the long-time limit of the diffusion coefficient does not exist.

We first check that  $D(s) = \frac{1}{4} \frac{\partial}{\partial s} \langle \Delta \mathbf{r}(s)^2 \rangle$  does not attain a stationary value but increases indefinitely as a function of time. Data for  $\varepsilon = 0.7$  are shown in Fig. 8 for a wide range of packing fractions. Obviously no stationary value is attained for any packing fraction; the same holds for other values of  $\varepsilon$ .

In order to check if one of the proposed time dependences in Eqs. (13) or (14) is correct, we plot  $D(s)/\ln(s)$  and  $D(s)/\sqrt{\ln(s)}$ . Similar to the test of the VACF, these quantities should fluctuate around a constant if they were describing  $D(s)$  correctly. The resulting graphs are plotted in Fig. 9.

Neither the prediction of MCT,  $D(t) \propto \sqrt{\ln(t)}$ , nor the prediction of hydrodynamics,  $D(t) \propto \ln(t)$ , account for the data in the full range of densities. MCT works slightly better at higher densities, whereas hydrodynamics fits the data better at intermediate densities. Hence, our data are not sufficient to discriminate between the two alternatives.

The above discussion shows that the long-time behavior in a two-dimensional fluid is not truly diffusive. On the other hand it is known that the long-time tails of the VACF are suppressed close to the glass transition, where the shear viscosity  $\nu$  increases dramatically. In fact, the MCT of Ernst *et al.* [25] predicts for a two-dimensional elastic fluid

$$\Phi(t) \propto \frac{kT}{8m\pi(\nu + D)} \frac{1}{t}. \quad (15)$$

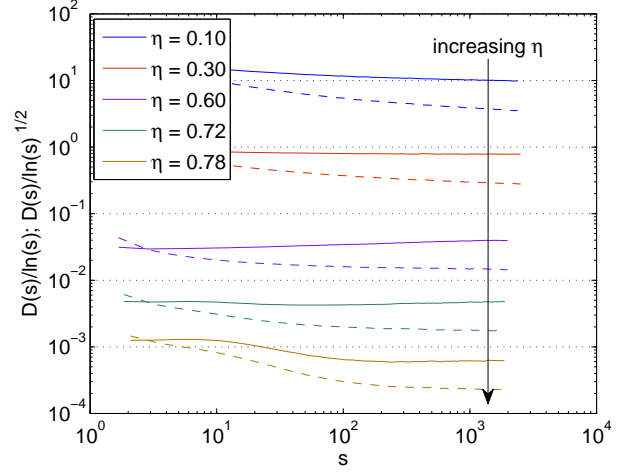


FIG. 9: (Color online) Full lines:  $D(s)/\ln(s)$ , dashed lines:  $D(s)/\sqrt{\ln(s)}$ .

For large packing fractions in the limit of the glass transition,  $\nu$  diverges and thus, the long-time tail in the VACF is suppressed. This allows us to calculate the diffusion coefficient approximately by two methods:

- We calculate the time dependent diffusion coefficient and estimate the diffusion coefficient by its value when the mean number of collisions per particle is  $s = 1000$ , *i.e.*,  $D = D(s = 1000)$ .
- We use a smaller system of  $N = 10^4$  particles where the long-time tails are cut off due to finite size effects. Hence the long-time limit of the integral over the VACF is constant and allows to extract the diffusion constant [30].

The diffusion coefficients extracted by these two different methods are depicted in Fig. 10. First, we note that the results of both methods agree quantitatively, so that it is indeed possible to estimate the diffusion coefficient from our data. Second, the diffusion coefficient decreases by several orders of magnitude as the glass transition is approached. Third, for more inelastic systems the decrease of  $D$  is shifted to higher densities.

#### D. Incoherent structure function

Complete information about the motion of a tagged particle is contained in the incoherent scattering function, defined as

$$S_{\text{inc}}(k, t) = \frac{1}{N} \sum_{i=1}^N \left\langle e^{i\mathbf{k} \cdot (\mathbf{r}_i(t) - \mathbf{r}_i(0))} \right\rangle. \quad (16)$$

In a molecular as well as in a colloidal glass, this function displays a two-step decay: The so called  $\beta$ -relaxation



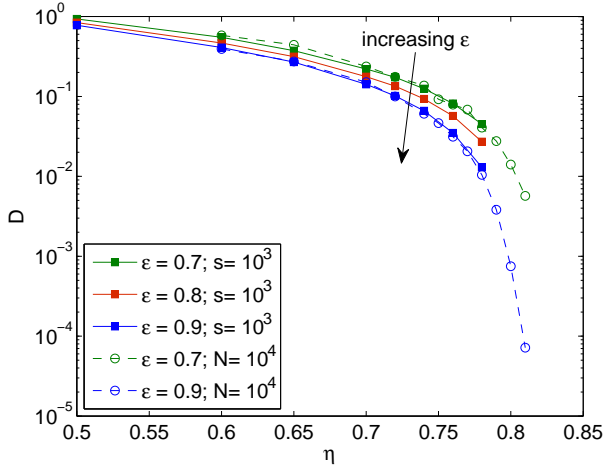


FIG. 10: (Color online) Diffusion coefficients for small particles extracted from the different data sets; for detailed explanation see text.

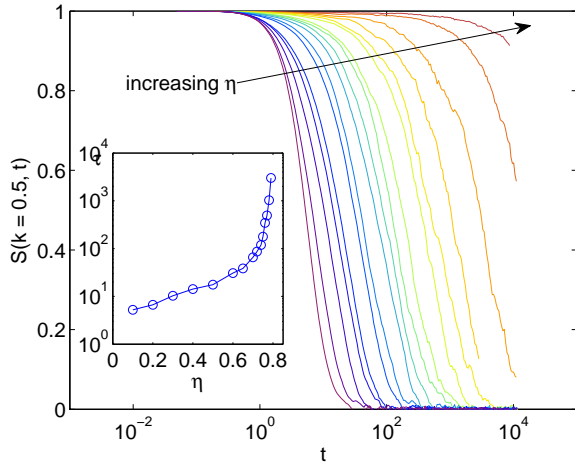


FIG. 11: (Color online)  $S_{\text{inc}}(k = 0.5, t)$  for small particles for  $\varepsilon = 0.90$  and different packing fractions  $\eta = 0.1; 0.2; 0.3; 0.4; 0.5; 0.6; 0.65; 0.7; 0.72; 0.74; 0.75; 0.76; 0.77; 0.78; 0.79; 0.80; 0.81$ . Inset: Relaxation time  $\tau$  at which the incoherent scattering function has decayed to half its initial value as a function of packing fraction.

towards a plateau and the subsequent  $\alpha$ -relaxation for asymptotically long times. The timescale of the  $\alpha$ -relaxation diverges as the glass transition is approached.

In Fig. 11, we plot the incoherent scattering function for  $\varepsilon = 0.9$  and increasing packing fraction up to  $\eta = 0.81$ . One clearly observes a pronounced slowing down which is quantified in the inset of Fig. 11. There we plot the relaxation time  $\tau(\eta)$ , the time at which  $S_{\text{inc}}(k = 0.5, t)$  has decayed to half its initial value. This relaxation time is seen to diverge as the glass transition is approached.

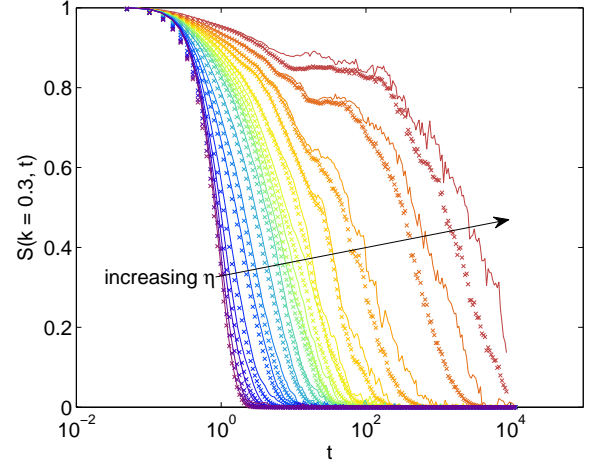


FIG. 12: (Color online)  $S_{\text{inc}}(k = 3, t)$  (full lines) for small particles in comparison to the Gaussian approximation (crosses); parameters as in Fig. 11

The two-step relaxation is related to the plateau in the MSD and hence more easily observed for larger wave numbers. We plot in Fig. 12 the incoherent scattering functions  $S_{\text{inc}}(k = 3, t)$  for various densities; a two-step relaxation is clearly observed for packing fractions  $\eta \geq 0.78$ . We also compare  $S_{\text{inc}}(k, t)$  to the Gaussian approximation

$$S_{\text{inc}}^{\text{Gauss}}(k, t) = e^{-k^2 \langle (\Delta \mathbf{r}(t))^2 \rangle / 4}. \quad (17)$$

As expected the Gaussian approximation works well for small densities at all times, whereas for the largest densities only the short time behaviour is approximately described by a Gaussian. The data for the incoherent scattering function look rather similar to those of the three-dimensional system which have been discussed in detail in [31].

### E. Dynamic heterogeneity

We expect the dynamics to become increasingly heterogeneous as the glass transition is approached. To demonstrate this point, we plot in Fig. 13 the MSD of the 10% slowest and 10% fastest particles as compared to an average over all particles in a system of packing fraction  $\eta = 0.8$  and  $\varepsilon = 0.9$ . Whereas the slow particles are completely immobile, the fast ones are seen to move diffusively covering distances which correspond to several radii. We plan to analyze dynamic heterogeneities in a future project.

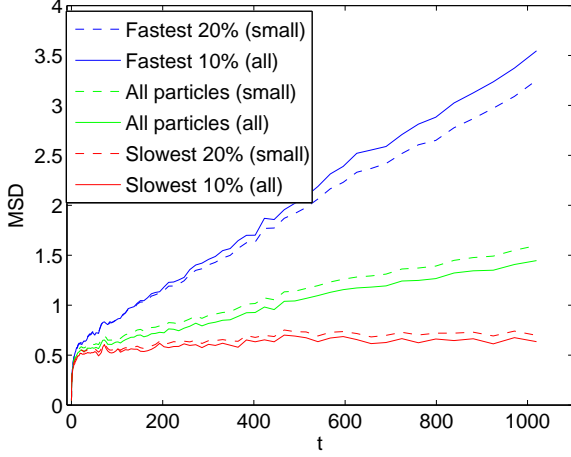


FIG. 13: (Color online) MSD for fast and slow particles, either restricted to small particles only (dashed) or for all particles (full line); the two upper curves refer to the fast particles, the two lower curves to the slow ones, and the two middle curves to all particles. The MSD at  $t = 10^3$  has been used to identify slow and fast particles.

### F. Pair correlation and structure factor

In this section we want to analyze the structure of a dense granular fluid and in particular exclude long range crystalline order. Translational order is detected by the pair correlation function,  $g(r)$ , which gives the probability to find a particle in a given distance  $r$ , from another particle at the origin:

$$g(r) = \frac{1}{n_0 N} \left\langle \sum_{j \neq i} \delta(\mathbf{r} - \mathbf{r}_{ij}) \right\rangle, \quad (18)$$

where  $n_0$  is number density. For a homogeneous system,  $g(r)$  approaches a constant as  $r \rightarrow \infty$  which is unity with the chosen normalization. Practically,  $g(r)$  is calculated as follows:

$$g(r) = \frac{1}{2\pi r \Delta r n_0 N} \left\langle \sum_{j \neq i} \theta(r + \Delta r - r_{ij}) \theta(r_{ij} - r) \right\rangle. \quad (19)$$

The bin size  $\Delta r = L/800$  has been chosen such that the number of bins and the average number of particles per bin remain constant for all packing fractions. This corresponds to  $\Delta r = 0.83$  for the most dilute ( $\eta = 0.1$ ) and  $\Delta r = 0.30$  for the densest ( $\eta = 0.81$ ) system.

For binary mixtures with big and small particles, there are three different pair correlation functions: between big particles only, between big and small particles, and between small particles only. All three radial distribution functions vanish for  $r/d_{ij} < 1$ , because the particles are hard, and have a global peak at the contact point,  $r/d_{ij} = 1$ . In Figs. 14 and 15 we show pair correlations for small and big particles with size ratio 1.25

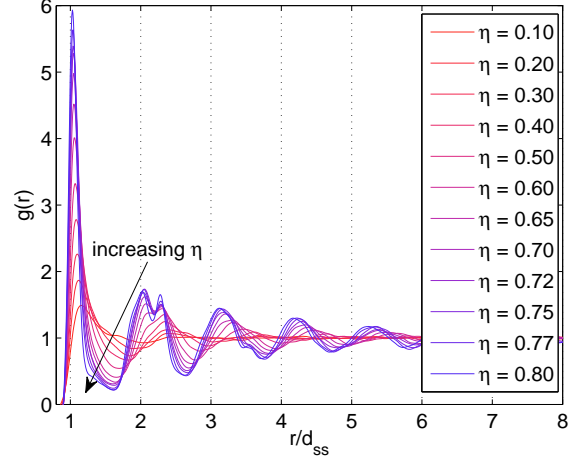


FIG. 14: (Color online) Pair correlation function for small particles for  $\varepsilon = 0.90$  and different packing fractions, where  $d_{ss}$  indicates the sum of two small particles' radii.

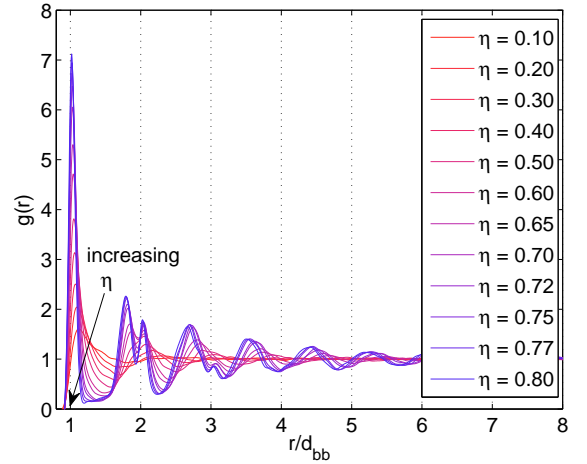


FIG. 15: (Color online) Pair correlation function for big particles for  $\varepsilon = 0.90$  and different packing fractions, where  $d_{bb}$  indicates the sum of two big particles' radii.

as a function of packing fraction. The data have been smoothed, implying a continuous growth of the correlations for small distances, whereas the raw data strictly vanish for  $r/d_{ij} < 1$ . Increasing the packing fraction, the peaks in  $g(r)$  get higher and sharper. Simultaneously oscillations develop for larger  $r$ . At packing fractions around  $\eta \sim 0.55$ , the second peak splits into two separate peaks, a phenomenon that is more pronounced for the big particles. This splitting of the second peak near  $r/d_{ij} = 2$  is a universal phenomena in glasses, but not a good indicator of the transition itself. Our results are in good agreement with the experimental ones of ref. [6].

We have chosen to study a bidisperse system in order



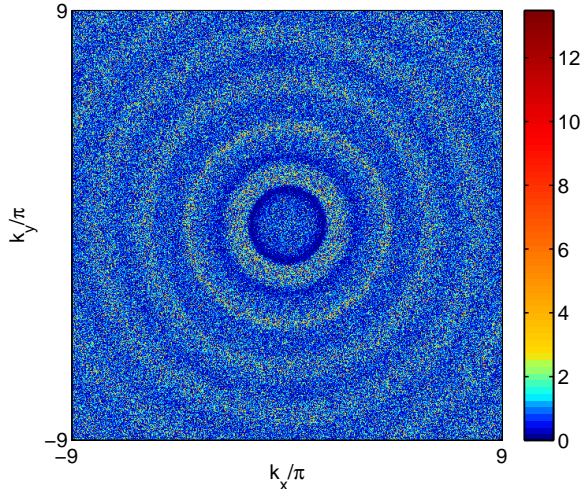


FIG. 16: (Color online) Structure factor for  $\varepsilon = 0.90$  and  $\eta = 0.81$ , for small particles. The contour plot of the structure factor shows a circular pattern which is characteristic of an amorphous system.

to avoid crystallization. Hence we need to verify that our system does indeed remain structurally disordered. We do so by mimicking a scattering experiment: We compute the static structure factor

$$S(\mathbf{k}) = \langle \rho_{\mathbf{k}}(t) \rho_{-\mathbf{k}}(t) \rangle, \quad (20)$$

where  $\mathbf{k}$  is the wave vector and  $\rho(\mathbf{k})$  is the collective density variable, defined as

$$\rho_{\mathbf{k}}(t) = \frac{1}{\sqrt{N}} \sum_{j=1}^N e^{i\mathbf{k} \cdot \mathbf{r}_j(t)}. \quad (21)$$

The computed structure factor is shown in Fig. 16 for the case of  $\varepsilon = 0.90$  and  $\eta = 0.80$ . The pattern is clearly isotropic, revealing the preferred distances which are visible as peaks in  $g(r)$ . We conclude that crystallization has been avoided and our system remains structurally disordered even when the particles – or a large fraction of them – are arrested.

An alternative measure ( $Q_6$ ) for orientational order was introduced in ref. [32] and applied to granular media in ref. [33]. We have computed  $Q_6$  for a range of packing fractions and find no indication of long range orientational order in agreement with ref. [33].

#### IV. CONCLUSION AND OUTLOOK

Simulations of a two-dimensional granular fluid in a stationary state reveal strong signatures of a glass tran-

sition, as the packing fraction is increased to approximately  $\eta = 0.8$ . The relaxation time of the incoherent scattering function diverges; the MSD develops a plateau; the diffusion constant goes to zero; the dynamics becomes increasingly heterogeneous. The results of event driven simulations are in qualitative agreement with recent experiments using vibro-fluidized [5] and air fluidized [6] granular systems.

We not only confirm the experimental results, but in addition investigate, how glassy dynamics depends on the degree of energy dissipation. In particular, we have tested the predictions of a recent mode-coupling theory [4] for the dependence of the glass transition on inelasticity. The theory predicts that the transition is pushed to higher densities the more inelastic the system is. To check this point, we have simulated a range of coefficients of restitution,  $0.5 \leq \varepsilon \leq 0.9$ , and compared the mean square displacements as a function of  $\varepsilon$ . The time  $\tau(\varepsilon, \eta)$ , where  $\langle \Delta \mathbf{r}^2(\tau) \rangle = 1$  is shifted to higher densities – in agreement with the theory. Similar behaviour is found for the lines of equal diffusivities. In addition to the shift in density, mode-coupling theory predicts that the plateau in the MSD is less pronounced for the more inelastic system. This prediction is also born out by our simulations.

Our simulations clearly show that the diffusion coefficient does not exist in a two-dimensional granular fluid; an appropriately defined time dependent diffusion coefficient grows indefinitely for long times. However, we are not able to extract the functional form unambiguously. The singular contribution is suppressed near the glass transition due to the divergence of the static shear viscosity, so that our estimates of the diffusion coefficient become increasingly more reliable as the glass transition is approached.

Dynamic heterogeneities have been investigated extensively in molecular glasses [34]. Various tools, such as multipoint correlations, have been used to detect increasing spatial correlations in a disordered structure. For the future, we plan to use these methods in order to analyze dynamic heterogeneities in a granular medium.

#### V. ACKNOWLEDGEMENTS

We thank Elmar Staerk and Matthias Sperl for providing us with initial configurations and Matthias Sperl, Timo Aspelmeier, Katharina Vollmayr-Lee, Felix Höfling and Till Kranz for many useful discussions. We furthermore acknowledge support from the DFG by FOR 1394.

- 
- [1] J. S. Olafsen and J. S. Urbach, *Phys. Rev. Lett.* **95**, 098002 (2005).
  - [2] P. M. Reis, R. A. Ingale, and M. D. Shattuck, *Phys. Rev. Lett.*, **96**, 258001 (2006).
  - [3] A. Liu and S. R. Nagel, *Nature (London)* **396**, 21 (1998).
  - [4] W. Till Kranz, M. Sperl, and A. Zippelius, *Phys. Rev. Lett.*, **104**, 225701 (2010).
  - [5] P. M. Reis, R. A. Ingale, and M. D. Shattuck, *Phys. Rev. Lett.*, **98**, 188301 (2007).
  - [6] A. R. Abate and D. J. Durian, *Phys. Rev. E* **74**, 031308 (2006).
  - [7] A. R. Abate and D. J. Durian, *Phys. Rev. E* **76**, 021306 (2007).
  - [8] L. Oger, C. Annic, D. Bideau, R. Dai and S. B. Savage, *J. Stat. Phys.*, **82**, 1047 (1996).
  - [9] B. J. Alder, and T. E. Wainwright, *Phys. Rev.* **127**, 359, (1962).
  - [10] A. C. Mitus, H. Weber, and D. Marx, *Phys. Rev. E* **55**, 6855, (1997).
  - [11] R. J. Speedy, *J. Chem. Phys.* **110**, 4559, (1998).
  - [12] D. R. M. Williams and F. C. MacKintosh, *Phys. Rev. E* **54**, R9 (1996).
  - [13] P. Espanol and P. Warren, *Europhys. Lett.* **30**, 191 (1995).
  - [14] B. D. Lubachevsky, *J. Comp. Phys.* **94**, 255 (1991).
  - [15] A. Fiege, T. Aspelmeier, A. Zippelius, *Phys. Rev. Lett.* **102**, 098001 (2009).
  - [16] E. Staerk and M. Sperl, unpublished 2011.
  - [17] A. Zippelius, *Physica A*, **369**, 143 (2006).
  - [18] C. Bizon, M. D. Shattuck, J. B. Swift, H. L. Swinney *et al.*, *Phys. Rev. E* **60**, 4340 (1999).
  - [19] M. Huthmann, A. Zippelius, *Phys. Rev. E* **56**, R6275 (1997).
  - [20] H. Uecker, W. T. Kranz, T. Aspelmeier, and A. Zippelius, *Phys. Rev. E*, **80**, 041303 (2009).
  - [21] B. J. Alder and T. E. Wainwright, *Phys. Rev. Lett.* **18**, 988 (1967).
  - [22] S. R. Williams, G. Bryant, I. K. Snook, and W. van Megen, *Phys. Rev. Lett.* **96**, 087801, (2006).
  - [23] M. Isobe, *Phys. Rev. E* **77**, 021201, (2008).
  - [24] J.-P. Hansen and I. R. McDonald, *Theory of Simple Liquids* (Academic Press, London, 1996).
  - [25] M. H. Ernst, E. H. Hauge, and J. M. J. van Leeuwen, *Phys. Rev. Lett.* **25**, 1254 (1970).
  - [26] T. E. Wainwright, B. J. Alder and D. M. Gass, *Phys. Rev. A* **4**, 233 (1971).
  - [27] K. Kawasaki, *Phys. Lett. A* **34**, 12 (1971).
  - [28] D. Forster, D. R. Nelson, and M. J. Stephen, *Phys. Rev. A* **16**, 732, (1977).
  - [29] M. P. Allen and D. J. Tildesley, *Computer Simulation of Liquids*, Oxford Science Publications (1987).
  - [30] F. Höfling, private communications, (2011).
  - [31] K. Vollmayr-Lee, T. Aspelmeier, and A. Zippelius, *Phys. Rev. E* **83**, 011301, (2011).
  - [32] P.J. Steinhardt, D.R. Nelson, and M. Ronchetti, *Phys. Rev. B* **28**, 784 (1983).
  - [33] S. Torquato, T. M. Truskett, and P. G. Debenedetti, *Phys. Rev. Lett.* **84**, 2064 (2000).
  - [34] L. Berthier, G. Biroli, *Rev. Mod. Phys.*, in press.